RESEARCH ARTICLE
SPACE PHYSICS: IONOSPHERE PHYSICS

Earth and Planetary Physics
1: 44-52, 2017
doi: 10.26464/epp2017006

A simulation study of 630 nm and 557.7 nm airglow variations due to dissociative recombination and thermal electrons by high-power HF heating

Tong Dang[1,2], JiuHou Lei[1,2,3*], XianKang Dou[1], and WeiXing Wan[4,5]

[1]CAS Key Laboratory of Geospace Environment, School of Earth and Space Sciences, University of Science and Technology of China, Hefei 230026, China;
[2]Mengcheng National Geophysical Observatory, University of Science and Technology of China, Hefei 230026, China;
[3]Collaborative Innovation Center of Astronautical Science and Technology, Harbin 150001, China;
[4]Institute of Geology and Geophysics, Chinese Academy of Sciences, Beijing 100029, China;
[5]University of Chinese Academy of Sciences, Beijing 100049, China

Abstract: One of the important effects of the ionospheric modification by high-power waves is the airglow enhancement. Both the thermal electrons and the dissociation recombination contribute to generate the airglow emissions during HF heating. However, the relative importance of the airglow emission induced by dissociative recombination and thermal electrons has been rarely investigated. In this study, we carry out a simulation study on the airglow produced by high-power HF heating at nighttime associated with dissociative recombination and thermal electrons. SAMI2 (Sami2 is Another Model of the Ionosphere) is employed to simulate the ionospheric variations during the HF heating. The main conclusions from this study are as follows: (1) For the airglow induced by dissociative recombination, both 630.0 nm and 557.7 nm emissions show a decrease at the heating wave reflection height during the heating period, while when the heating is turned off, an increase is shown at lower altitudes. The reduction of airglow during the heating is caused by the rapid increase of electron temperature and the diffusion of plasmas dominates the after-heating airglow enhancement. (2) 630.0 nm emission due to thermal electrons is greatly enhanced at the wave reflection height, indicating that thermal electrons play a major role in exciting 630.0 nm emission. For the 557.7 nm emission, the excitation threshold (4.17 eV) is too high for thermal electrons. (3) The combined effect of dissociative recombination and thermal electrons could be the possible reason for the observed X-mode (extraordinary mode) suppression of 630.0 nm airglow during O-mode (ordinary mode) enhancement.

Keywords: airglow; thermal electron; dissociative recombination; HF heating

Citation: Dang, T., J. H. Lei., X. K. Dou., and W. X. Wan (2017). A simulation study of 630 nm and 557.7 nm airglow variations due to dissociative recombination and thermal electrons by high-power HF heating. *Earth Planet. Phys.*, *1*, 44-52. http://doi.org/10.26464/epp2017006

1. Introduction

Strong airglow enhancements have been observed during high-power HF heating since 1970s (Biondi et al., 1970; Sipler et al., 1974; Bernhardt et al., 1988; Brändström et al., 1999; Djuth et al., 2005; Gustavsson et al., 2005; Kosch et al., 2005; Holma et al., 2006). The red and green line emissions (630.0 and 557.7 nm) of atomic oxygen are among the most prominent features during the HF heating experiments. The natural 630.0 nm and 557.7 nm airglow in the ionosphere is produced by the excitation through dissociative recombination of oxygen molecule ions by collision with electrons (e.g., Peterson et al., 1966; Bates, 1992).

The greatly enhanced airglow observed during the heating experiments has been suggested to be caused by the accelerated electrons (Perkins and Kaw, 1971; Weinstock and Bezzerides, 1974; Weinstock and Sleeper, 1975; Gurevich et al., 1985) and the thermal electrons (Mantas, 1994; Mantas and Carlson, 1996). The theory of accelerated electrons suggested that the enhanced excitation of O(^1D) is due to a non-thermal electron distribution in the energy range above 2 eV. The source of this distribution is the acceleration of electrons by Langmuir turbulence (Gordon and Carlson, 1974; Meltz and Perkins, 1974; Gurevich et al., 1985; Bernhardt et al., 1989).

The other hypothesis is that the red-line airglow is caused by direct excitation of oxygen atoms by collision with thermal electrons through the high energy tail of a Maxwellian electron distribution. Mantas (1994) suggested that the thermal electron excitation of the O(^1D) state is sufficient to explain the 630.0 nm emission intensity observed during the ionosphere heating experiments. Later, Mishin et al. (2000) suggested that the Maxwellian electron distribution should be corrected for the effects of N_2 inelastic collisions.

Correspondence to: J. H. Lei, leijh@ustc.edu.cn
Received 25 JUL 2017; Accepted 11 AUG 2017.
Accepted article online 29 AUG 2017.

Although the airglow variations during HF heating were widely examined, the comparison of the airglow emission induced by dissociative recombination and thermal electrons has rarely been investigated. In this work, we mainly focus on the 630.0 nm and 557.7 nm airglow caused by dissociative recombination reaction and thermal electrons. We utilize SAMI2 (Sami2 is Another Model of the Ionosphere) to simulate the ionospheric variations during the HF heating by including an additional heating source, with a time step of 30 seconds. Based on the model, we present the comparison of the spatial and temporal variations of airglow emission induced by the dissociative recombination and thermal electrons. The thermal electrons effect under the condition of non-Maxwellian electron distribution is also discussed.

2. Models Description

2.1 Heating Model

In this study, we use the ionospheric model SAMI2 (Huba et al., 2000) to conduct heating simulations with a realistic ionosphere. SAMI2 solves plasma continuity, momentum, and energy equations to provide plasma densities and temperatures. The plasma field-aligned motion along a magnetic flux tube and the motion across the flux tube via $\boldsymbol{E}\times\boldsymbol{B}$ drift are considered in the model. The neutral species are specified using the Mass Spectrometer Incoherent Scatter model (MSIS00) and the Horizontal Wind Model (HWM93). SAMI2 (together with the 3D version SAMI3) has been used in a number of simulation studies of ionospheric artificial heating (e.g., Wu TW et al., 2012; Zawdie et al., 2013, 2015; Zawdie and Huba, 2014).

Similar to Wu TW et al. (2012), we add a source term ($Q_{\rm RF}$) in the electron temperature equation. The modified electron temperature equation is

$$\frac{\partial T_e}{\partial t}-\frac{2}{3}\frac{1}{n_e k}b_s^2\frac{\partial}{\partial s}\kappa_e\frac{\partial T_e}{\partial s}=Q_{\rm en}+Q_{\rm ei}+Q_{\rm phe}+Q_{\rm RF}. \quad (1)$$

The second term on the left-hand side is the heat conduction term, κ_e is the parallel electron thermal conductance, k is the Boltzmann constant, and b_s is the component of the magnetic field in the field line direction. The other heating/cooling terms on the right-hand side of equation (1) are associated with electron-neutral collisions ($Q_{\rm en}$), electron-ion collisions ($Q_{\rm ei}$), and photoelectron heating ($Q_{\rm phe}$). $Q_{\rm RF}$ is the heating term, which is represented by a Gaussian-shaped source:

$$Q_{\rm RF}=\left(\frac{{\rm d}T_e}{{\rm d}t}\right)_0\exp\left[-(z-z_0)^2/\Delta z^2\right]\exp\left[-(\theta-\theta_0)^2/\Delta\theta^2\right], \quad (2)$$

where $\left(\frac{{\rm d}T_e}{{\rm d}t}\right)_0$ is the total heating rate per electron in K/s, z is the altitude, and θ is the latitude. z_0 and θ_0 are the center altitude and latitude of the heating location and Δz and $\Delta\theta$ stand for the altitudinal and latitudinal extent of the heating region. In this study, we set the total heating rate $\left(\frac{{\rm d}T_e}{{\rm d}t}\right)_0$ to be 1000 K/s, which is suggested in previous studies using the SURA heater (Milikh et al., 2010a). The location of the HF heater is set at Arecibo, Puerto Rico (18.3°N, 66.7°W, 28°N magnetic latitude). HF heating begins at 01:00 LT and lasts for 5 min. In this study, Δz=10 km and $\Delta\theta$=0.05°, which are the same as Wu TW et al. (2012). The pump frequency is 5 MHz, corresponding to the wave reflection height of 282 km and electron density of 3.1×10^5 cm^{-3} above Arecibo Observatory at 01:00 LT. The wave reflection height is below the F region peak height of about 300 km.

2.2 Airglow Model

The 630.0 nm and 557.7 nm optical emissions in the ionosphere are produced by oxygen atoms in radiative transitions O(^1D->^3P) and O(^1S->^1D), respectively. The main sources of O(^1D) and O(^1S) are dissociative recombination.

$$O_2^+ + e \rightarrow O(^1D,^1S)+O(^3P). \quad (3)$$

To estimate the airglow induced by dissociative recombination, we use the airglow model proposed by Vlasov et al. (2005), which includes the effects of molecular ions. The volume emission rate (VER) of red- and green-line emission are given by the formulae

$${\rm VER_R}=\frac{A_{1D}\left\{\mu_D\alpha_{O_2^+}[O_2^+]n_e+\frac{\beta\alpha_{NO^+}[NO^+]n_e\gamma_D[O_2]}{\gamma_D[O_2]+\gamma_O[O]}\right\}}{k_1[N_2]+k_2[O_2]+k_3[O]+A_{1D}+A_{2D}}, \quad (4)$$

$${\rm VER_G}=\frac{A_{1S}\mu_S\alpha_{O_2^+}[O_2^+]n_e}{A_{1S}+A_{2S}}, \quad (5)$$

where β is the yield of the N(^2D) atoms in the reaction between NO^+ and electron; γ_O is the rate coefficient of the deactivation of N(^2D) atoms by atomic oxygen; γ_D is the rate coefficient of reaction between N(^2D) and O_2; k_1, k_2, and k_3 are the rate coefficient of O(^1D) quenching by N_2, O_2, and O, respectively; A_{1D} and A_{2D} are the O(^1D)->O(^3P) transition coefficients; A_{1S} and A_{2S} are the O(^1S)->O(^1D) transition coefficients. The parameters and reactions are described in detail in Vlasov et al. (2005).

During the HF heating, the excited oxygen state O(^1D) could be generated through the impact of thermal electrons:

$$O(^3P)+e^*\rightarrow O(^1D)+e, \quad (6)$$

where e^* denotes the electrons with energy greater than 1.96 eV. For the 557.7 nm airglow, the threshold energy of O(^1S) state is 4.17 eV. In this study, we use the airglow model proposed in Mantas (1994) and Gurevich and Milikh (1997) to calculate the airglow excited by thermal electrons:

$${\rm VER_R^*}=\frac{A_{1D}k_{ex}^{(1)}[O]n_e}{k_1[N_2]+k_2[O_2]+k_3[O]+A_{1D}+A_{2D}}, \quad (7)$$

$${\rm VER_G^*}=A_{1S}k_{ex}^{(2)}[O]n_e. \quad (8)$$

Here $k_{ex}^{(1)}$ and $k_{ex}^{(2)}$ are respectively the excitation rates of O(^1D) and O(^1S), which are defined as

$$k_{ex}^{(1)}=0.5\sqrt{T_e}\frac{9329+T_e}{(51813+T_e)^3}\exp\left(-\frac{22756}{T_e}\right)({\rm cm^3/s}), \quad (9)$$

$$k_{ex}^{(2)}=0.2\sqrt{T_e}\frac{19960+T_e}{(114080+T_e)^3}\exp\left(-\frac{48390}{T_e}\right)({\rm cm^3/s}). \quad (10)$$

Finally, the integrated airglow intensity can be expressed as

$$I=10^{-6}\int_0^\infty {\rm VER}(z)\,{\rm d}z. \quad (11)$$

The main purpose of this work is to investigate the relative effect of dissociative recombination and thermal electrons on airglow. We run SAMI2 simulation in the meridional plane of Arecibo under the following geophysical conditions: $F_{10.7}$=100, Ap=4, and day of year = 130. Electron density, electron temperature and the calculated airglow without HF heating are subtracted for each grid point and time step to show the heating induced perturbations.

3. Results and Discussions

Figure 1 shows the perturbations of electron temperature and density at the end time of HF heating (01:05 LT) as a function of latitude and altitude. As given in Figure 1a, after 5 min of heating, electron temperature shows a large enhancement, with field-aligned striations extending from 150 km to above 500 km. Electron temperature reaches maximum at the heating center region, about 2100 K above the ambient temperature. As shown in Figure 1b, a density depletion of about 1×10^5 cm^{-3} can be seen at the heating center region, while electron density has an increase above and below the heating center region. This structure is possibly associated with the large thermal pressure due to the absorption of heating waves at the wave reflection height. Plasma tends to diffuse along the field line under the force of the pressure gradient. Note that the electron density perturbation is asymmetric on the two sides of the heating center region along the field line. The altitude above the heating center exhibits a higher density increase than the lower altitudes, which is probably due to the low diffusion coefficient as well as the high recombination rate at low altitudes. Such field-aligned density ducts have been observed by the Detection of Electro-Magnetic Emissions Transmitted from Earthquake Regions (DEMETER) and Defense Meteorological Satellite Program (DMSP) satellites routinely in the topside ionosphere during ionospheric modification experiments at the High Frequency Active Auroral Research Program (HAARP) and SURA heating facilities (Milikh et al., 2008, 2010b; Rapoport et al., 2010; Fallen et al., 2011).

Figure 2 presents temporal variations of electron temperature and density along the magnetic field line. The zero time represents the start of artificial heating, and thus the heating ends at 5 min. Electron temperature greatly enhances during the heating period and rapidly depletes in 1-2 minutes. For electron density, as heating starts, a density cavity forms along with the density enhancement on both sides. Different from the electron temperature changes, due to the large time constant of diffusion transport process, the electron density takes more than 30 min to recover to the preconditions. The variations of electron temperature and density by HF-pump heating are confirmed by previous studies (e.g., Hansen et al., 1989; Milikh et al., 2010a, 2010b, 2012).

Figure 3 shows the volume emission rate changes of red-line (left) and green-line (right) airglow at 01:01 LT, 01:04 LT, and 01:07 LT. After 1 min of heating (01:01 LT), the intensities of both red-line and green-line airglow show a decrease at the heating center region along the field line. As compared with the large extension of electron temperature and density, the airglow perturbation mainly focuses on the reflection height around 260–320 km. At a later time of 4 min (01:04 LT), the decrease of airglow became weaker. When the heating has been turned off for 2 min (01:07 LT), the airglow shows an increase at a lower altitude than the heating center, which is in contrast with the airglow change during the heating period. The change of the 557.7 nm airglow is similar to that of the 630.0 nm airglow with a smaller perturbation of about 0.7 cm^{-3}s^{-1}.

The above simulation shows that the airglow decreases when the transmitter was turned on while increases when the transmitter was turned off. This behavior is usually prominent when the heater was run with extraordinary mode (X-mode) polarization (Biondi et al., 1970; Sipler and Biondi, 1972). The X-mode polarization wave collisionally heats the plasma without parametric excitation of electrostatic waves (Bernhardt et al., 1988). As shown by equations (4) and (5), the volume emission rate of airglow is mainly dominated by the dissociative recombination coefficient α and electron density (α is approximately proportional to $T_e^{-0.6}$). Con-

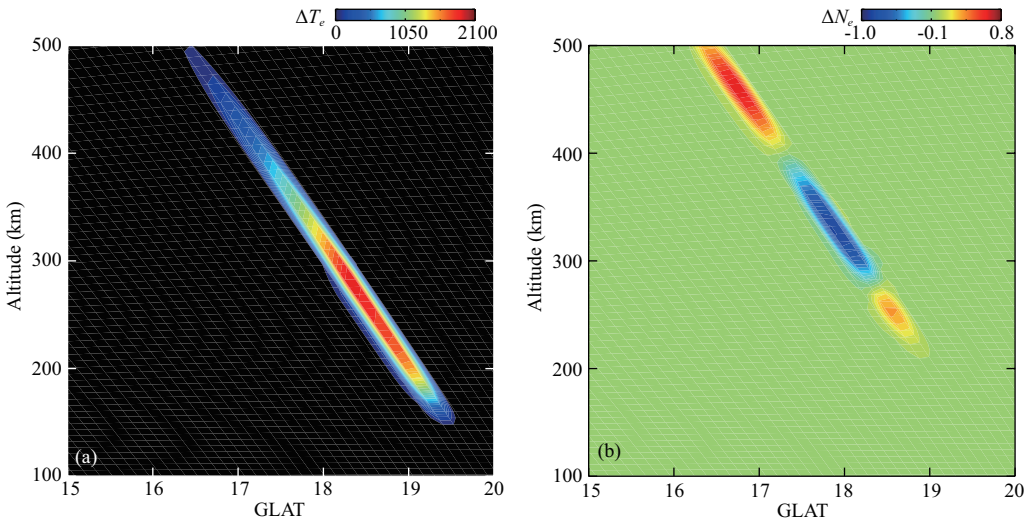

Figure 1. Variations of electron temperature (in units of K) and electron density (in units of 10^5 cm^{-3}) as a function of geographic latitude and altitude at the end of the heating duration.

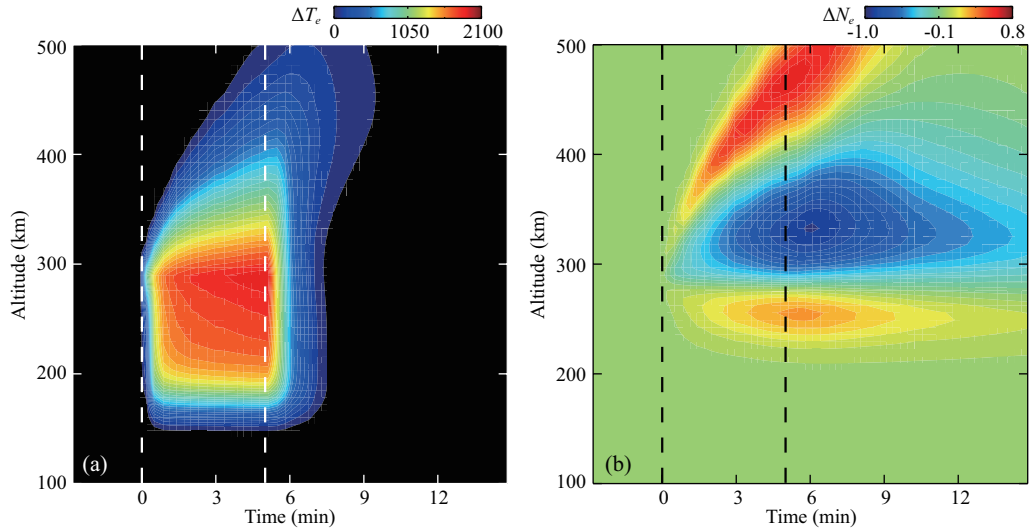

Figure 2. Temporal changes of (a) electron temperature (in units of K) and (b) electron density (in units of 10^5 cm^{-3}) along the magnetic field line around the heated region. The dashed lines represent the start time and end time of the HF heating.

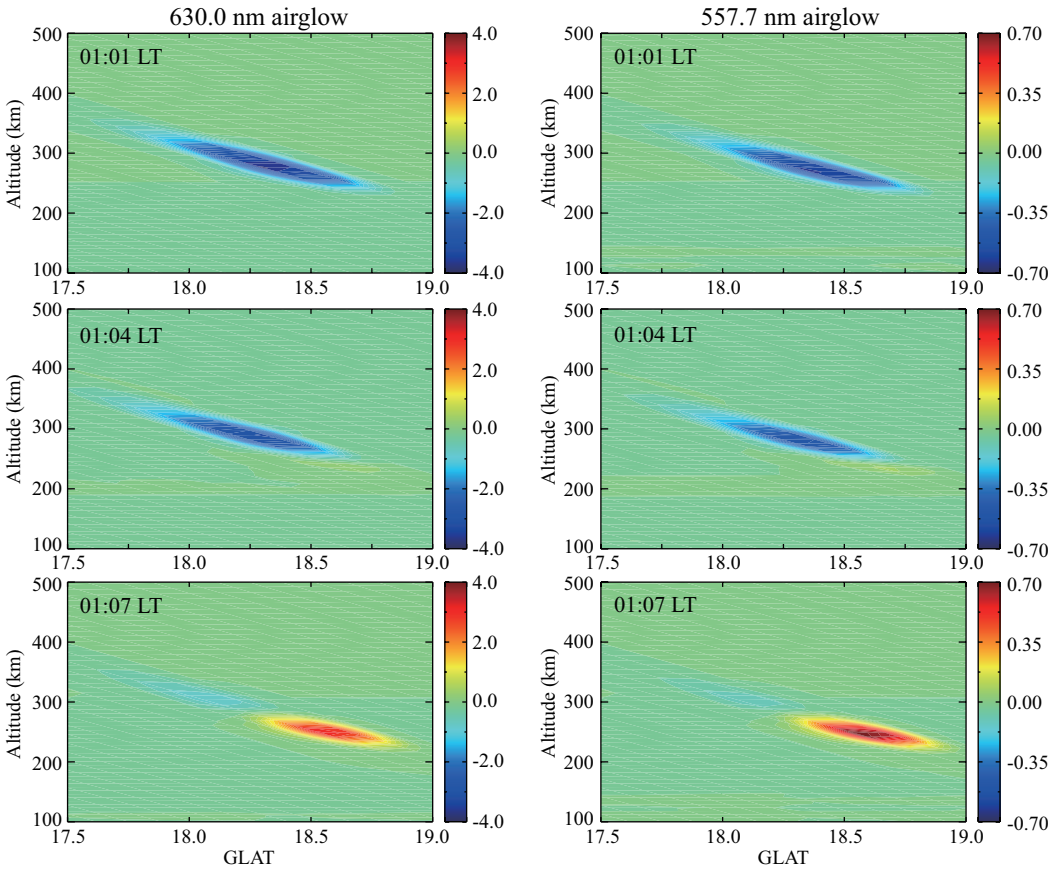

Figure 3. Perturbations of the volume emission rate (in units of $cm^{-3}s^{-1}$) of (left) red-line and (right) green-line airglow due to dissociative recombination as a function of geographic latitude and altitude.

sequently, when the electron temperature increases significantly during the heating period, X-mode heating suppresses the airglow intensity by reducing the recombination coefficient. This suppression of the natural airglow is usually masked by collisional excitation during O-mode heating. When the heating is terminated, the electron temperature rapidly depletes to unperturbed condition; however, the electron density change could last for a long time. Therefore, the airglow perturbation is mainly dominated by the variations of electron density when the heater is turned off. Electrons at the heating region are transported to lower altitudes along the field line (Figure 1b), and thus the airglow enhances at a lower height. Note that a weak depletion at

01:07 LT also occurs at the wave reflection region because of the electron density cavity.

Then, we take the thermal electrons into account to investigate the enhanced airglow during the ordinary mode (O-mode) heating. Figure 4 shows the changes of volume emission rate due to thermal electrons as a function of geographic latitude and altitude. Strong 630.0 nm airglow increase can be noted at the heating time of 1 min (01:01 LT). As the HF heating continues, the volume emission rate of red-line airglow increases up to 50 $cm^{-3}s^{-1}$ at 01:04 LT. After the heating is turned off in the bottom panel, the airglow enhancement is depleted. For the green-line airglow, the variation of volume emission rate due to the thermal electron is much smaller than that caused by the recombination effect, indicating that the thermal electrons induced 557.7 nm airglow is weak. This is associated with the high threshold energy (4.17 eV) for the excitation of O(^1S).

The temporal variations of airglow along the heated magnetic field line are displayed in Figure 5. Both the red-line and green-line airglows decrease during the heating, but increase when the heating is turned off. The strongest reduction happens when the heating is turned on and the strongest enhancement occurs at 2 min after the heating is terminated. The magnitude of green-line airglow changes is much smaller than that of the red-line airglow. For the 630.0 nm airglow induced by thermal electrons in the bottom panel, the volume emission rate largely enhances at the reflection height as the heating starts and disappears in 1 min after heating is turned off. The volume emission rate of the red-line airglow reaches 50 $cm^{-3}s^{-1}$ when the HF heating is absent. As compared with Figure 5b, the green-line airglow due to thermal electrons in Figure 5d is negligible, although it shows a slight increase during heating period.

In Figure 6, the variations of airglow intensity integrated by the volume emission rate are shown. The recombination associated red-line airglow intensity has a decrease of 20 Rayleighs (R) during the heating period and has an increase up to 10 R after 2 min as the heating is switched off. The airglow intensity induced by the thermal electrons strongly increases and peaks with a value of 270 R when the heating is terminated. After that, the airglow rapidly recovers to the precondition level in about 1 min. As compared with the red-line airglow, the green-line intensity is much smaller. The 557.7 nm airglow intensity caused by the recombination effect shows a similar variation as the red-line airglow but with smaller magnitude. The maximum reduction and enhancement are 4 R and 2 R, respectively. The intensity of green-line airglow caused by thermal electrons is almost negligible. Gustavsson et al. (2009) presented an interesting observation of 630 nm emission from HAARP heater with simultaneous transmission in X and O-mode. They firstly reported the additional transmission of X-mode significantly suppressed the enhancement of O-mode 630.0 nm enhancement. This result is consistent with our calculations and might be associated with the combined effect of dissociative recombination and thermal electrons. Here it should be

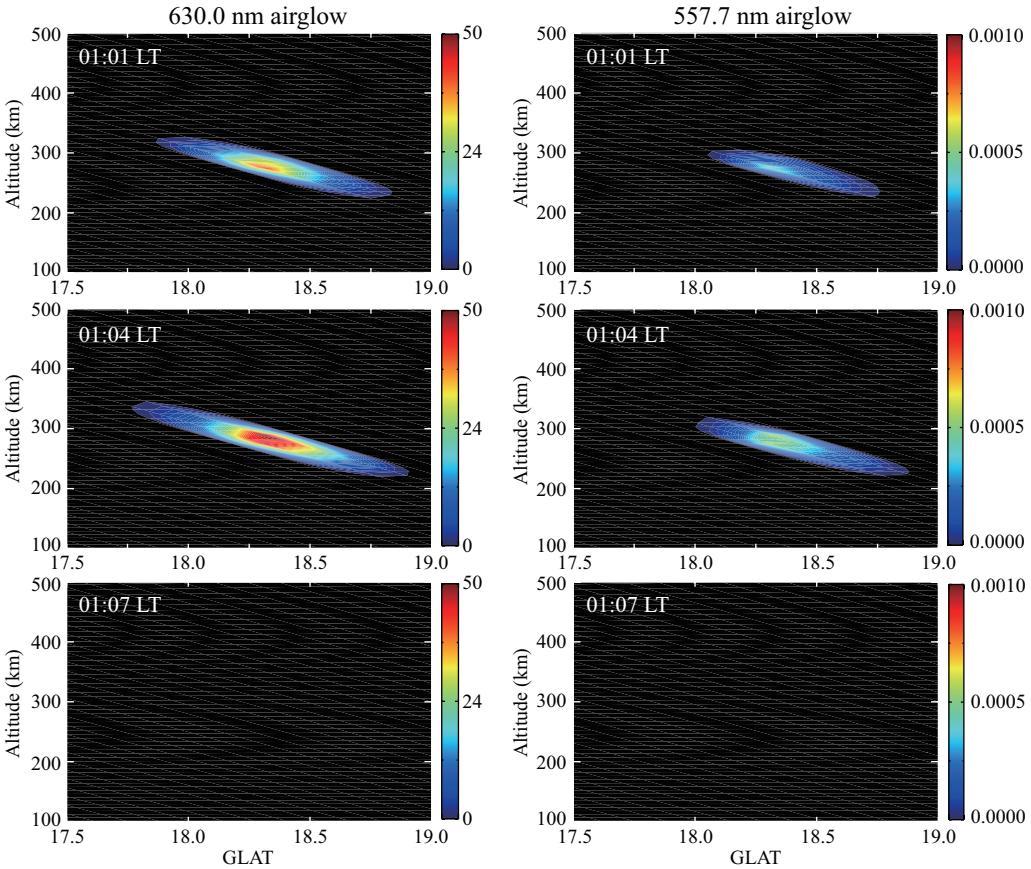

Figure 4. Similar to Figure 3, but for the effect of thermal electrons.

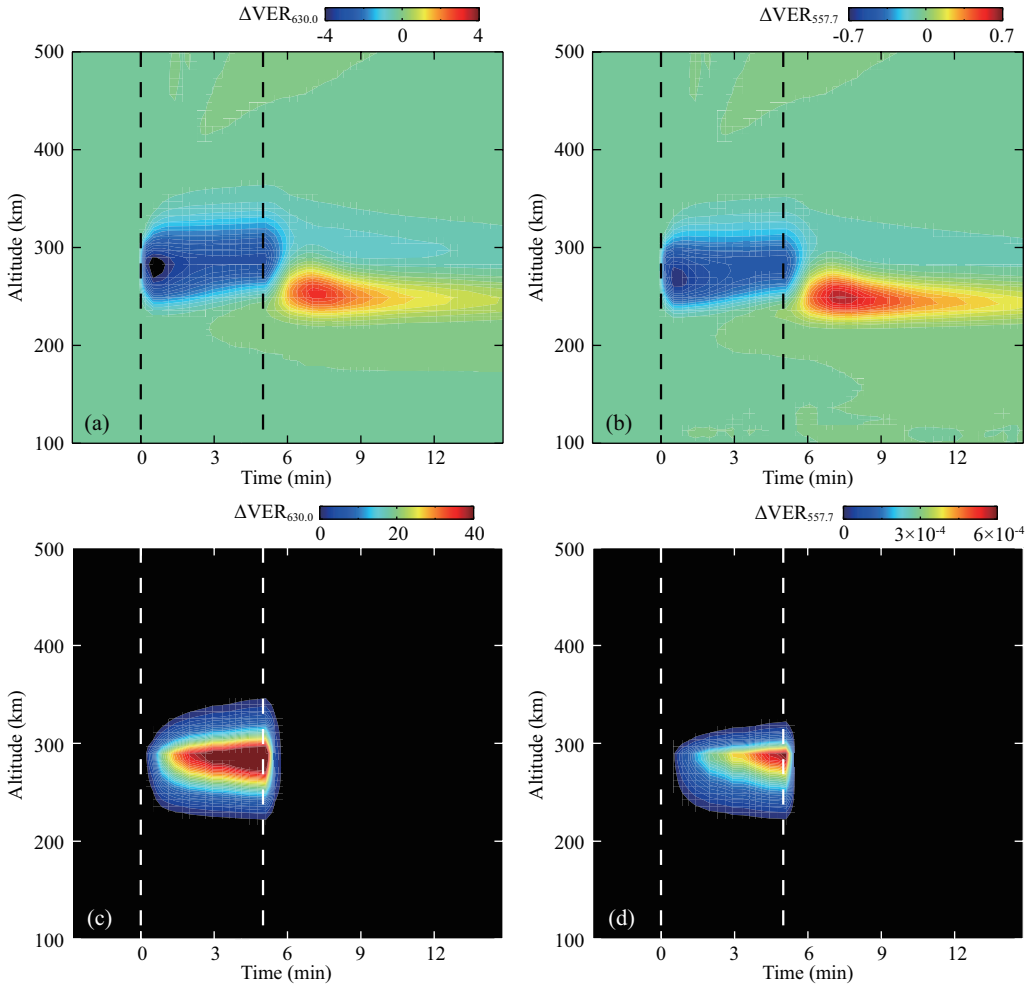

Figure 5. Temporal variations of volume emission rate (in units of $cm^{-3}s^{-1}$) of (left) red-line and (right) green-line emission along the magnetic field line due to (upper) the dissociative recombination effect and (bottom) thermal electrons. The dashed lines represent the start time and end time of the HF heating. Note different color ranges are used in each subplot.

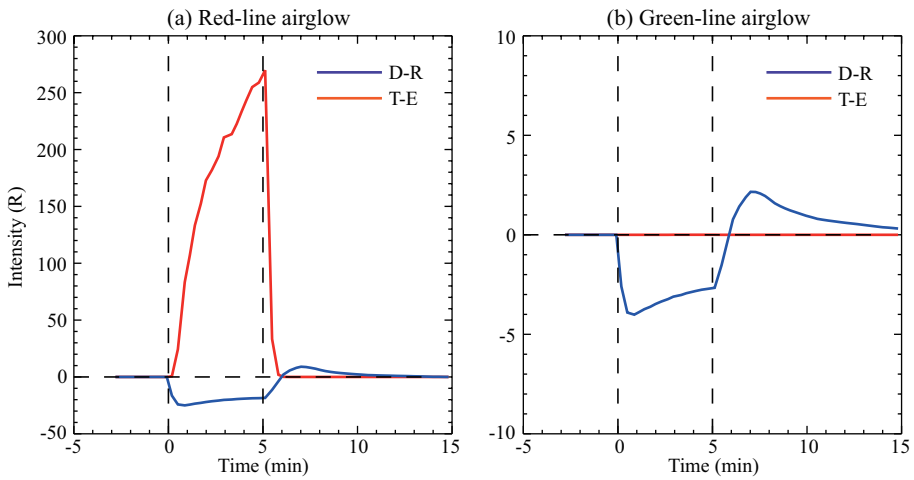

Figure 6. Temporal variations of (a) red-line and (b) green-line intensity along the heated field line due to dissociative recombination (D-R) and thermal electrons (T-E). The vertical dashed lines represent the start time and end time of the HF heating.

pointed out that the integrated airglow intensity is calculated along the magnetic field, and thus it may be overestimated.

Over the years, strong enhancement of optical emissions from states with excitation threshold higher than 1.96 eV of O(^1D) has been observed. These emissions involve 557.7 nm (with excitation threshold energy of 4.17 eV) (e.g., Bernhardt et al., 1989; Gust-

avsson et al., 2002), 660.0 nm (9 eV) (Djuth et al., 1999), 844.6 nm (10.99 eV) (Gustavsson et al., 2005), and 427.8 nm (18.75 eV) (Gustavsson et al., 2001; Holma et al., 2006). From our simulation results of the green-line airglow, the theory of thermal electrons is unable to explain the emissions with excitation threshold energy of 4.17 eV or higher. The suprathermal electrons, which have been suggested to be accelerated by Langmuir turbulence or the upper hybrid plasma turbulence, are a widely accepted theory for these emissions (e.g., Grach, 1999; Mishin et al., 2005; Gurevich, 2007). The relative contributions of accelerated electrons, thermal electrons and dissociative recombination to the airglow require further investigation.

Despite of the strong red-line airglow enhancement, Sergienko et al. (2000) shows that the thermal electron theory significantly overestimates the observed emission intensity. Mishin et al. (2000) and Gustavsson et al. (2004) further proposed that the collisions between N_2 and electrons lead to a strong depletion from the Maxwellian electron distribution in the high energy range. Consequently, this depletion results in a reduction of O(^1D) state and airglow intensity. Next, we carry out a simple sensitivity analysis of airglow due to deviations from the Maxwellian electron distribution. The standard Maxwellian electron energy distribution is

$$F_{\mathrm{M}}(E) = 2\sqrt{\frac{E}{\pi}}\left(\frac{1}{kT}\right)^{\frac{3}{2}}\exp\left(\frac{-E}{kT}\right), \tag{12}$$

where T is the electron temperature, k is the Boltzmann constant, and E is the electron energy. Through solving the one dimensional Vlasov equation for ionospheric F-region conditions during high-power HF-heating, Wang JG et al. (1997) found that the energy distribution of suprathermal electrons induced by HF heating could be modeled by a power law. Vlasov et al. (2004) found that the electron energy distribution in the energy range of 2-3 eV can deviate significantly from a Maxwellian distribution due to the impact of N_2 vibrational excitation. In this study, the effect of deviation from the Maxwellian electron energy distribution on the airglow intensity is tested using the combination of the results from Wang JG et al. (1997) and Vlasov et al. (2004). The non-Maxwellian electron energy distribution F_{NM} is expressed as

$$F_{\mathrm{NM}}(E) = \begin{cases} F_{\mathrm{M}}\exp\left[\left(\frac{1}{2T_e} - \left\{\frac{1}{4T_e^2} + \frac{R}{2T_eE'_{\mathrm{av}}}\right\}^{\frac{1}{2}}\right)E'\right], & 2 \leqslant E \leqslant 3\mathrm{eV} \\ 3.11\times10^{-3}\left(\frac{T_e}{E}\right)^{0.85}, & E \geqslant 3\mathrm{eV} \end{cases} \tag{13}$$

where R=1.2, E'=E-2 eV and E'_{av}=0.5 eV. Figure 7 shows the comparison of Maxwellian and non-Maxwellian electron energy distributions at the electron temperature of 4000 K. The non-Maxwellian electron energy distribution function $F_{\mathrm{NM}}(E)$ is lower than the pure thermal one $F_{\mathrm{M}}(E)$ in the energy range between 2 eV and 3 eV, but higher in the energy range greater than 3 eV. The simulated airglow difference between Maxwellian and non-Maxwellian electron energy is shown in Figure 8. The volume emission rate of red-line airglow under the modified non-Maxwellian electron distribution is about 6 cm^{-3}s^{-1} lower than the pure thermal case at around 300 km. The depletion in the energy range between 2-3 eV of

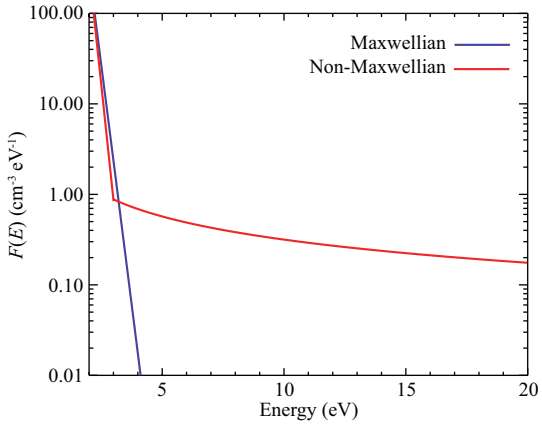

Figure 7. Comparison of Maxwellian and non-Maxwellian electron energy distributions.

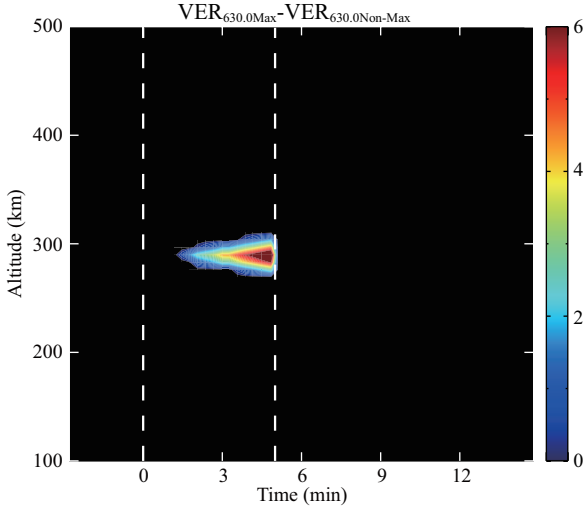

Figure 8. Difference of volume emission rates (in units of cm^{-3}s^{-1}) of 630.0 nm airglow between Maxwellian and non-Maxwellian electron energy distributions shown in Figure 7.

Maxwellian electron distribution causes a smaller airglow intensity than the pure thermal model. This test supports the assumption in Sergienko et al. (2000) that the inelastic collisions between N_2 and electrons lead to an overestimation of the airglow intensity in the pure thermal theory. In addition, the present calculation does not consider excitation of O(^1D) and O(^1S) through collisions with other excited species, such as N_2 rotational and vibrational states. The non-Maxwellian component with energies of 20 eV may produce many excited species that can also contribute to excite O(^1D) and O(^1S) through collisions (e.g., Rees, 1963; Banks et al., 1974) and thus the results in this study might be influenced.

4. Conclusions

In this study, we present the simulation results of the heating effect on 630.0 nm and 557.7 nm airglow based on SAMI2. We mainly focus on the comparison of airglow caused by the dissociative recombination reaction and thermal electrons during the nighttime. The main results are summarized as follows:

(1) The intensities of both 630.0 nm and 557.7 nm airglow induced by the dissociative recombination show a decrease during the heating and increase after the heating is turned off. The intensity perturbation of the 630.0 nm airglow is about 15 R larger than that of 557.7 nm airglow.

(2) The volume emission rate of airglow due to dissociative recombination shows significant altitudinal and temporal distributions. During the heating period, the reduction of recombination coefficient, which is caused by the increase of electron temperature, leads to a decrease of airglow at the wave reflection height. When the heating is turned off, the field-aligned downward diffusion of electron dominates the airglow variation and enhances the airglow at lower altitudes.

(3) During the heating period, 630.0 nm emission is greatly enhanced by 260 R at wave reflection height due to thermal electrons, indicating that the thermal process plays a major role in causing 630.0 nm emission. The enhancement rapidly depletes in 1 min after the heating is turned off. The 557.7 nm emission induced by thermal electrons is nearly unchanged because of the high excitation threshold energy (4.17eV) of O(^1S). The theory of accelerated electron could probably explain the observed green-line enhancement.

Acknowledgments

Please contact Tong Dang (dangt@mail.ustc.edu.cn) for model outputs used in this paper. The SAMI2 ionosphere model was writtenanddevelopedbytheNavalResearchLaboratory(http://www.nrl.navy.mil/ppd/branches/6790/sami2). This work was supported by the National Natural Science Foundation of China (41325017, 41274158, 41274157, and 41421063), the fundamental research funds for the central universities, and Thousand Young Talents Program of China.

References

Banks, P. M., Chappell, C. R., and Nagy, A. F. (1974). A new model for the interaction of auroral electrons with the atmosphere: Spectral degradation, backscatter, optical emission, and ionization. *J. Geophys. Res.*, *79*(10), 1459-1470. https://doi.org/10.1029/JA079i010p01459

Bates, D. R. (1992). Nightglow emissions from oxygen in the lower thermosphere. *Planet. Space Sci.*, *40*(2), 211-221. https://doi.org/10.1016/0032-0633(92)90059-W

Bernhardt, P. A., Duncan, L. M., and Tepley, C. A. (1988). Artificial airglow excited by high-power radio waves. *Science*, *242*(4881), 1022-1027. https://doi.org/10.1126/science.242.4881.1022

Bernhardt, P. A., Tepley, C. A., and Duncan, L. M. (1989). Airglow enhancements associated with plasma cavities formed during Ionospheric Heating Experiments. *J. Geophys. Res.*, *94*(A7), 9071-9092. https://doi.org/10.1029/JA094iA07p09071

Biondi, A. A., Sipler, D. P., and Hake Jr, R. D. (1970). Optical (λ6300) detection of radio frequency heating of electrons in the F region. *J. Geophys. Res.*, *75*(31), 6421-6424. https://doi.org/10.1029/JA075i031p06421

Brändström, B. U. E., Leyser, T. B., Steen, Å., Rietveld, M. T., Gustavsson, B., Aso, T., and Ejiri, M. (1999). Unambiguous evidence of HF pump-enhanced airglow at auroral latitudes. *Geophys. Res. Lett.*, *26*(23), 3561-3564. https://doi.org/10.1029/1999GL010693

Djuth, F. T., Bernhardt, P. A., Tepley, C. A., Gardner, J. A., Kelley, M. C., Broadfoot, A. L., Kagan, L. M., Sulzer, M. P., Elder, J. H., Selcher, C., Isham, B., Brown, C., and Carlson, H. C. (1999). Large airglow enhancements produced via wave-plasma interactions in sporadic E. *Geophys. Res. Lett.*, *26*(11), 1557-1560. https://doi.org/10.1029/1999GL900296

Djuth, F. T., Pedersen, T. R., Gerken, E. A., Bernhardt, P. A., Selcher, C. A., Bristow, W. A., and Kosch, M. J. (2005). Ionospheric modification at twice the electron cyclotron frequency. *Phys. Rev. Lett.*, *94*(12), 125001. https://doi.org/10.1103/PhysRevLett.94.125001

Fallen, C. T., Secan, J. A., and Watkins, B. J. (2011). In-situ measurements of topside ionosphere electron density enhancements during an HF-modification experiment. *Geophys. Res. Lett.*, *38*(8), L08101. https://doi.org/10.1029/2011GL046887

Gordon, W. E., and Carlson Jr, H. C. (1974). Arecibo heating experiments. *Radio Sci.*, *9*(11), 1041-1047. https://doi.org/10.1029/RS009i011p01041

Grach, S. M. (1999). On kinetic effects in the ionospheric F-region modified by powerful radio waves. *Radiophys. Quantum Electron.*, *42*(7), 572-588. https://doi.org/10.1007/bf02677563

Gurevich, A. V., Dimant, Y. S., Milikh, G. M., and Vas'kov, V. V. (1985). Multiple acceleration of electrons in the regions of high-power radio-wave reflection in the ionosphere. *J. Atmos. Terr. Phys.*, *47*(11), 1057-1070. https://doi.org/10.1016/0021-9169(85)90023-6

Gurevich, A. V., and Milikh, G. M. (1997). Artificial airglow due to modifications of the ionosphere by powerful radio waves. *J. Geophys. Res.*, *102*(A1), 389-394. https://doi.org/10.1029/96JA02916

Gurevich, A. V. (2007). Nonlinear effects in the ionosphere. *Physics-Uspekhi*, *50*(11), 1091-1121. https://doi.org/10.1070/PU2007v050n11ABEH006212

Gustavsson, B., Sergienko, T., Rietveld, M. T., Honary, F., Steen, A., Brändström, B. U. E., Leyser, T. B., Aruliah, A. L., Aso, T., Ejiri, M., and Marple, S. (2001). First tomographic estimate of volume distribution of HF-pump enhanced airglow emission. *J. Geophys. Res.*, *106*(A12), 29105-29123. https://doi.org/10.1029/2000JA900167

Gustavsson, B., Brändström, B. U. E., Steen, Å., Sergienko, T., Leyser, T. B., Rietveld, M. T., Aso T., and Ejiri, M. (2002). Nearly simultaneous images of HF-pump enhanced airglow at 6300 Å and 5577 Å. *Geophys. Res. Lett.*, *29*(24), 73-1. https://doi.org/10.1029/2002GL015350

Gustavsson, B., Sergienko, T., Häggström, I., Honary, F., and Aso, T. (2004). Simulation of high energy tail of electron distribution function. *Adv. Polar Upper Atmos. Res.*, *18*, 1-9.

Gustavsson, B., Sergienko, T., Kosch, M. J., Rietveld, M. T., Brändström, B. U. E., Leyser, T. B., Isham, B., Gallop, P., Aso, T., Ejiri, M., Grydeland, T., Steen, Å., LaHoz, C., Kaila, K., Jussila, J., and Holma, H. (2005). The electron energy distribution during HF pumping, a picture painted with all colors. *Ann. Geophys.*, *23*(5), 1747-1754. https://doi.org/10.5194/angeo-23-1747-2005

Gustavsson, B., Newsome, R., Leyser, T. B., Kosch, M. J., Norin, L., McCarrick, M., Pedersen, T., and Watkins, B. J. (2009). First observations of X-mode suppression of O-mode HF enhancements at 6300 Å. *Geophys. Res. Lett.*, *36*(20), L20102. https://doi.org/10.1029/2009GL039421

Hansen, J. D., Morales, G. J., and Maggs, J. E. (1989). Daytime saturation of thermal cavitons. *J. Geophys. Res.*, *94*(A6), 6833-6840. https://doi.org/10.1029/JA094iA06p06833

Holma, H., Kaila, K. U., Kosch, M. J., and Rietveld, M. T. (2006). Recognizing the blue emission in artificial aurora. *Adv. Space Res.*, *38*(11), 2653-2658. https://doi.org/10.1016/j.asr.2005.07.036

Huba, J. D., Joyce, G., and Fedder, J. A. (2000). Sami2 is Another Model of the Ionosphere (SAMI2): A new low-latitude ionosphere model. *J. Geophys. Res.*, *105*(A10), 23035-23053. https://doi.org/10.1029/2000ja000035

Kosch, M. J., Pedersen, T., Rietveld, M. T., Gustavsson, B., Grach, S. M., and Hagfors, T. (2005). Artificial optical emissions in the high-latitude thermosphere induced by powerful radio waves: An observational review. *Adv. Space Res.*, *40*(3), 365-376. https://doi.org/10.1016/j.asr.2007.02.061

Mantas, G. P. (1994). Large 6300-Å airglow intensity enhancements observed in Ionosphere Heating Experiments are excited by thermal electrons. *J. Geophys. Res.*, *99*(A5), 8993-9002. https://doi.org/10.1029/94JA00347

Mantas, G. P., and Carlson, H. C. (1996). Reinterpretation of the 6300-Å airglow enhancements observed in ionosphere heating experiments based on analysis of Platteville, Colorado, data. *J. Geophys. Res.*, *101*(A1), 195-209. https://doi.org/10.1029/95JA02760

Meltz, G., and Perkins, F. W. (1974). Ionospheric modification theory: Past, present, and future. *Radio Sci.*, *9*(11), 885-888.

https://doi.org/10.1029/RS009i011p00885

Milikh, G. M., Papadopoulos, K., Shroff, H., Chang, C. L., Wallace, T., Mishin, E. V., Parrot, M., and Berthelier, J. J. (2008). Formation of artificial ionospheric ducts. *Geophys. Res. Lett.*, *35*(17), L17104. https://doi.org/10.1029/2008GL034630

Milikh, G. M., Demekhov, A. G., Papadopoulos, K., Vartanyan, A., Huba, J. D., and Joyce, G. (2010a). Model for artificial ionospheric duct formation due to HF heating. *Geophys. Res. Lett.*, *37*(7), L07803. https://doi.org/10.1029/2010GL042684

Milikh, G. M., Mishin, E., Galkin, I., Vartanyan, A., Roth, C., and Reinisch, B. W. (2010b). Ion outflows and artificial ducts in the topside ionosphere at HAARP. *Geophys. Res. Lett.*, *37*(18), L18102. https://doi.org/10.1029/2010GL044636

Milikh, G. M., Demekhov, A., Vartanyan, A., Mishin, E. V., and Huba, J. (2012). A new model for formation of artificial ducts due to ionospheric HF-heating. *Geophys. Res. Lett.*, *39*(10), L10102. https://doi.org/10.1029/2012GL051718

Mishin, E., Carlson, H. C., and Hagfors, T. (2000). On the electron distribution function in the F region and airglow enhancements during HF modification experiments. *Geophys. Res. Lett.*, *27*(18), 2857-2860. https://doi.org/10.1029/2000GL000075

Mishin, E., Burke, W., and Pedersen, T. (2005). HF-induced airglow at magnetic zenith: theoretical considerations. *Ann. Geophys.*, *23*(1), 47-53. https://doi.org/10.5194/angeo-23-47-2005

Perkins, F. W., and Kaw, P. K. (1971). On the role of plasma instabilities in ionospheric heating by radio waves. *J. Geophys. Res.*, *76*(1), 282-284. https://doi.org/10.1029/JA076i001p00282

Peterson, V. L., VanZandt, T. E., and Norton, R. B. (1966). F-region nightglow emissions of atomic oxygen: 1. Theory. *J. Geophys. Res.*, *71*(9), 2255-2265. https://doi.org/10.1029/JZ071i009p02255

Rapoport, V. O., Frolov, V. L., Polyakov, S. V., Komrakov, G. P., Ryzhov, N. A., Markov, G. A., Belov, A. S., Parrot, M., and Rauch, J. L. (2010). VLF electromagnetic field structures in ionosphere disturbed by Sura RF heating facility. *J. Geophys. Res.*, *115*(A10), A10332. https://doi.org/10.1029/2010JA015484

Rees, M. H. (1963). Auroral ionization and excitation by incident energetic electrons. *Planet. Space Sci.*, *11*(10), 1209-1218. https://doi.org/10.1016/0032-0633(63)90252-6

Sergienko, T., Gustavsson, B., Steen, Å., Brändström, U., Rietveld, M., Leyser, T. B., and Honary, F. (2000). Analysis of excitation of the 630.0 nm airglow during a heating experiment in Tromsø on February 16, 1999. *Phys. Chem. Earth Part B Hydrol. Oceans Atmos.*, *25*(5-6), 531-535. https://doi.org/10.1016/S1464-1909(00)00059-9

Sipler, D. P., and Biondi, M. A. (1972). Measurements of O (^1D) quenching rates in the F region. *J. Geophys. Res.*, *77*(31), 6202-6212. https://doi.org/10.1029/JA077i031p06202

Sipler, D. P., Enemark, E., and Biondi, M. A. (1974). 6300-Å intensity variations produced by the Arecibo Ionospheric Modification Experiment. *J. Geophys. Res.*, *79*(28), 4276-4280. https://doi.org/10.1029/JA079i028p04276

Vlasov, M. N., Kelley, M. C., and Gerken, E. (2004). Impact of vibrational excitation on ionospheric parameters and artificial airglow during HF heating in the F region. *J. Geophys. Res.*, *109*(A9), A09304. https://doi.org/10.1029/2003JA010316

Vlasov, M. N., Nicolls, M. J., Kelley, M. C., Smith, S. M., Aponte, N., and González, S. A. (2005). Modeling of airglow and ionospheric parameters at Arecibo during quiet and disturbed periods in October 2002. *J. Geophys. Res.*, *110*(A7), A07303. https://doi.org/10.1029/2005JA011074

Wang, J. G., Newman, D. L., and Goldman, M. V. (1997). Vlasov simulations of electron heating by Langmuir turbulence near the critical altitude in the radiation-modified ionosphere. *J. Atmos. Sol. Terr. Phys.*, *59*(18), 2461-2474. https://doi.org/10.1016/S1364-6826(96)00140-X

Weinstock, J., and Bezzerides, B. (1974). Theory of electron acceleration during parametric instabilities. *Phys. Rev. Lett.*, *32*(14), 754-758. https://doi.org/10.1103/PhysRevLett.32.754

Weinstock, J., and Sleeper, A. M. (1975). Theory of enhanced ion and electron heating, and dissipation, due to ion acoustic turbulence. *Phys. Fluids.*, *18*(2), 247-250. https://doi.org/10.1063/1.861110

Wu, T. W., Huba, J. D., Joyce, G., and Bernhardt, P. A. (2012). Modeling Arecibo conjugate heating effects with SAMI2. *Geophys. Res. Lett.*, *39*(7), L07103. https://doi.org/10.1029/2012GL051311

Zawdie, K. A., Huba, J. D., and Wu, T. W. (2013). Modeling 3-D artificial ionospheric ducts. *J. Geophys. Res.*, *118*(11), 7450-7457. https://doi.org/10.1002/2013JA018823

Zawdie, K. A., and Huba, J. D. (2014). Can HF heating generate ESF bubbles?. *Geophys. Res. Lett.*, *41*(23), 8155-8160. https://doi.org/10.1002/2014GL062293

Zawdie, K. A., Huba, J. D., Drob, D. P., and Bernhardt, P. A. (2015). A coupled ionosphere-raytrace model for high-power HF heating. *Geophys. Res. Lett.*, *42*, 9650-9656. https://doi.org/10.1002/2015GL066673